J Eng Math (2016) 97:147–159
DOI 10.1007/s10665-015-9802-1

Modified intrinsic extended finite element method for elliptic equation with interfaces

Jianping Zhao · Yanren Hou · Lina Song

Received: 23 April 2014 / Accepted: 27 April 2015 / Published online: 28 July 2015

Abstract In this paper, a modified intrinsic extended finite element method (XFEM) for one-dimensional and two-dimensional elliptic equations with discontinuous coefficients and interfaces is proposed. We improve the intrinsic XFEM by changing the shape functions of the critical nodes. The improved shape functions can be used to catch the discontinuous information near interfaces. In addition, we modify the Gauss integration in special elements cut by interfaces. Numerical experiments are presented to verify the feasibility and superiority of the modified intrinsic XFEM compared with the standard FEM and extrinsic XFEM for this type of problem. Results also show that the modified intrinsic XFEM can generate an approximate solution whose error is $O(h^2)$ in an L^2-norm and $O(h)$ in an energy norm if the Q1 element is used.

Keywords Extended finite element method · Generalized finite element method · Interface · Intrinsic

Mathematics Subject Classification 65N30 · 35Q10

1 Introduction

We consider a boundary value problem of the form

$$\begin{cases} -\nabla \cdot (a(x, y)\nabla u(x, y)) = f(x, y) & (x, y) \in \Omega \backslash \Gamma, \\ u(x, y) = 0 & (x, y) \in \partial\Omega, \end{cases} \tag{1}$$

J. Zhao (✉)
College of Mathematics and System Sciences, Xinjiang University, Urumqi 830046, China
e-mail: zhaojianping@126.com

J. Zhao
Xinjiang Institute of Ecology and Geography, Chinese Academy of Sciences, Urumqi 830011, China

Y. Hou
School of Mathematics and Statistics, Xi'an Jiaotong University, Xi'an, China
e-mail: yrhou@xjtu.edu.cn

L. Song
College of Mathematics, Qingdao University, Qingdao 266071, China

where Ω is a bounded domain in $\mathbb{R}^d$ $(d = 2, 3)$ with polygonal or polyhedral boundary $\partial\Omega$, $f \in L^2(\Omega)$, $\Gamma = \bigcup_i \Gamma_i$ is the internal interface that may consist of several pieces of local internal interfaces Γ_i, which are also called interfaces henceforth. Generally, any two different interfaces might be intersected, that is, $\Gamma_i \cap \Gamma_j \neq \emptyset\, (i \neq j)$ is possible. The function $a(x, y) \in L^\infty(\Omega)$ satisfies

$$0 < \alpha \leq a(x, y) \leq \beta < \infty \quad \forall (x, y) \in \Omega,$$

where α and β are constants. Assume that the function $a(x, y)$ is discontinuous across the interface Γ_i, while it is continuous away from the interfaces. Assume the discontinuous functions of u and $a(x, y)\partial u/\partial n$ are $\hat{v}(x, y)$ and $\hat{w}(x, y)$:

$$\begin{cases} [u(x, y)] = \hat{v}(x, y) & (x, y) \in \Gamma, \\ \left[a(x, y)\frac{\partial u}{\partial n}\right] = \hat{w}(x, y) & (x, y) \in \Gamma. \end{cases} \tag{2}$$

This interface problem appears in fluid dynamics and materials science. The common methods [i.e., finite difference method (FDM) and finite element method (FEM)] fail to solve such problems owing to the singularities of the interface. It is essential to improve the common methods for this kind of interface problem.

For the approximation of nonsmooth solutions, there are two fundamental approaches. One approach is to refine the discretization near the critical regions. Remeshing is required in this case, i.e., placing more grid points along the interface and around the intersection. This strategy involves a posteriori error estimates. For examples, Cai and Zhang [1] proposed recovery-based error estimators, and Bernardi and Verfùrth [2] proposed weighted-residual error estimators to deal with interface problems. Another approach is to enrich a polynomial approximation space such that the nonsmooth solutions can be modeled independently of the mesh. For example, the immersed boundary method (IBM) [3] and the immersed interface method (IIM) [4–12] were developed on the basis of finite difference methods, which modify the standard centered difference approximation to maintain second-order accuracy or to obtain higher-order methods, while the immersed interface finite element method (IIFEM) [13–15] is designed to cope with interface problems based on finite elements.

Meanwhile, a variety of modifications to the conventional FEM have been made within the framework of the partition of unity (PU). A typical example is the extended finite element method (XFEM). It was first realized in [16] by Belytschko and Black by enriching the nodes of finite elements near crack tips and along crack surfaces with asymptotic crack tip functions. Since then, such methods have received wide attention, and fast progress has been made with them [17–27]. However, the stiffness matrix of the XFEM could be severely ill-conditioned, and the ill-conditioning is much worse than in the standard FEM [28]. Use of the XFEM would entrail a severe loss of accuracy when computing the associated linear system.

Based on the development of these methods, we try to use the intrinsic XFEM [25] to solve elliptic problems with complex interfaces, such as interfaces intersecting with each other. No additional unknowns are introduced at the nodes contained in elements intersected by interfaces. The intrinsic XFEM often involves using the moving least squares (MLS) method for construction of special, enriched shape functions. The condition number of stiff matrices of the XFEM is much greater than that of the FEM because MLS moment matrices are added. In this paper, we modify the ordinary intrinsic XFEM in two ways. First, instead of the MLS function, we change the critical shape function in those elements that are cut by interfaces. The special shape functions are discontinuous piecewise linear polynomials. According to this modification, the shape function contains the information on the interface. Moreover, the special shape functions build different PUs over each subdomain of Ω, and they satisfy the connection conditions of the interface in (1). Second, to obtain a sufficiently accurate integration, we use a modified integration in elements cut by interfaces and a standard Gaussian integration in other elements. The condition number of the final stiff matrix retains the same order as the standard FEM.

The rest of the paper is organized as follows. Section 2 introduces preliminary definitions related to the XFEM and the weak form of (1). The modified intrinsic XFEM is proposed in Sect. 3. The integration strategy for XFEM is discussed in Sect. 4, and a numerical experiment is presented in Sect. 5 to show the feasibility of the proposed algorithms. Finally, conclusions are drawn in Sect. 6.

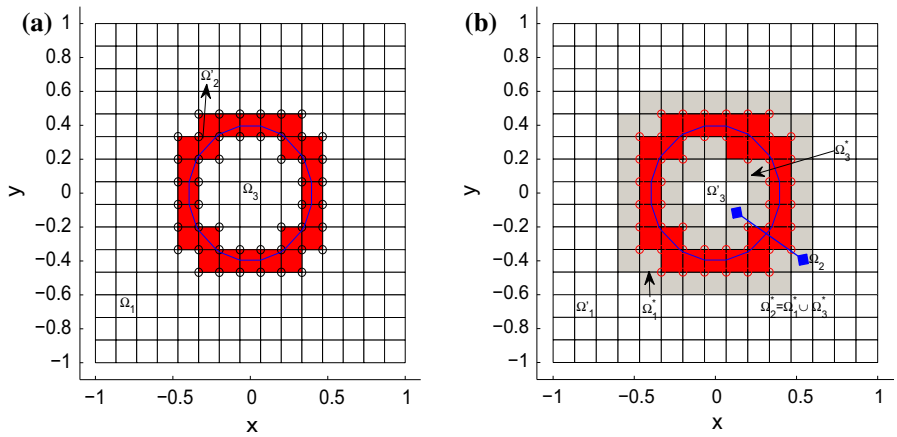

Fig. 1 Decomposition of domain Ω into subdomains Ω_l' and Ω_l^*, $\Omega_l = \Omega_l' \cup \Omega_l^*$ $(1 \le l \le 3)$, $\Gamma : x^2 + y^2 = r^2$. **a** Ω_1, Ω_3, Ω_2', **b** Ω_2, Ω_1', Ω_3', Ω_l^*. (Color figure online)

2 Preliminary definitions

We use the standard notations for Sobolev spaces $H^k(\Omega\backslash\Gamma) := W^{k,2}(\Omega)$ and their associated norm $\|\cdot\|_{H^k(\Omega)}$ and seminorm $|\cdot|_{H^k(\Omega)}$, especially $H^0(\Omega) := L^2(\Omega)$.

If the connection is $\hat{v} = 0$ and $\hat{w} = 0$, then the weak formulation of (1) reads as follows: find $u \in H_0^1(\Omega)$ such that

$$B(u, v) := \int_\Omega a(x, y)\nabla u \cdot \nabla v \, \mathrm{d}x \, \mathrm{d}y = \int_\Omega f v \, \mathrm{d}x \, \mathrm{d}y = (f, v) \quad \forall v \in H_0^1(\Omega). \tag{3}$$

Since $a(x, y)$ is bounded and away from zero, the variational problem has a unique solution.

We consider a uniform rectangular partition of Ω, whose set of all element nodes is denoted by I. We decompose the set I into m nodal subsets I_l, which satisfy $I = \bigcup_{l=1}^m I_l$ and $I_i \cap I_j = \emptyset, \quad \forall i \ne j$.

For a given I_l, we introduce its relative subdomains Ω_l, Ω_l', and $\Omega_l^\star$, and Ω_l denotes the union of all elements sharing the vertex x_i for all $i \in I_l$.

That is, $\Omega_l := \bigcup_{i \in I_l} D^i$, where D^i denotes the union of elements possessing the vertex x_i, $\Omega_l^\star$ is the subset of Ω_l and denotes the elements in Ω_l but also shares other vertices x_j $(j \in I \setminus I_l)$.

Moreover, $\Omega_l^\star := \bigcup_{s \in M \setminus l \Omega_l \bigcap \Omega_s}$ where $M = \{1, 2, \ldots, m\}$. Then $\Omega_l' = \Omega_l - \Omega_l^\star$. It is obvious that Ω_l consists only of elements possessing the vertex $\{x_i\}$, $i \in I$.

It becomes obvious from Fig. 1 that the subdomains Ω_l' neither overlap nor have any shared boundaries with each other, whereas the transition elements belong to at least two subdomains Ω_l^*. Different PUs may be constructed over each of the subdomains Ω_l with respect to the nodal sets I_l, respectively. For example, in the interface problem in 1, in Ω_1 and Ω_3, a standard FE shape function can be used. However, special enriched shape functions are proposed in Ω_2 where the solution is highly discontinuous across the interface Γ. Our main idea is to construct an intrinsic shape function for the elliptic equation with a complicated interface.

3 Modified intrinsic extended finite element method

The approximate solution can be written in the following form:

$$u^h(x) = \sum_{i \in I} u_i \tilde{N}_i(x), \tag{4}$$

where the $\tilde{N}_i(x)$ are special shape functions. If the problem is continuous, then the polynomial approximation space is adequate, that is, $\tilde{N}_i(x) := N_i(x)$ are the standard FEM shape functions. However, if the problem is discontinuous or

weakly discontinuous, the special shape functions are used so that they are able to capture discontinuities. Similarly, the method can be used to enrich the solution with singularity or other known characteristics. Of course, we need to ensure $\{\tilde{N}_i(x)\}$ divide into partition of union, that is, $\sum_i \tilde{N}_i(x) = 1$. Then the numerical scheme of (3) can be written as follows: find $u^h(x)$ such that

$$B(u^h(x), \widetilde{N}_j(x)) = (f, \widetilde{N}_j(x)) \quad \forall j.$$

Let ω_i be the impact domain of node x_i. The set $\{\omega_i\}$ is the open cover set of Ω. It can be divided into two cases.

If ω_i is far from the interface Γ, we can use a standard FEM shape function as the corresponding shape function $\tilde{N}_i(x) = N_i(x)$.

If $\omega_i \cap \Gamma \neq \emptyset$, we suppose that the nodes (x^*, y_{j_1}) and (x_{i_1}, y^*) are the intersections of Γ with the element $[x_{i_1}, x_{i_1+1}] \times [y_{j_1}, y_{j_1+1}]$. It can be fixed by the following expressions:

$$\begin{cases} \phi(x, y^*) = 0 \quad x = x_{i_1}, & \text{(5a)} \\ \phi(x^*, y) = 0 \quad y = y_{j_1}. & \text{(5b)} \end{cases}$$

We can use a special shape function that is fixed by the information of the discontinuous interface:

$$\big[u\big] = 0, \quad \big[a(x, y)\tfrac{\partial u}{\partial n}\big] = 0.$$

For convenience, we transfer the element domain $E_i = [x_{j_1-1}, x_{j_1+1}] \times [y_{j_2-1}, y_{j_2+1}]$ to a reference element $[-1, 1]^2$ by linear transformation,

$$\xi = \tfrac{x - x_{j_1}}{h}, \quad \xi \in [-1, 1], \qquad \eta = \tfrac{y - y_{j_2}}{h}, \quad \eta \in [-1, 1]. \tag{6}$$

First, we consider the shape function for the x-axis in the reference interval $[-1, 1]$. If there is a discontinuous interface ξ^* corresponding to the original element $\xi^* = (x^* - x_{j_1})/h$, and $[u]|_{x^*} = 0$, $\big[a(x, y)\tfrac{\partial u}{\partial n}\big] = 0$, then

$$u^+_{\xi^*} = u^-_{\xi^*}, \quad a^+ u^+_x\Big|_{\xi^*} = a^- u^-_x\Big|_{\xi^*}. \tag{7}$$

Second, we can solve the new shape function $\tilde{N}_i(x)$ using a piecewise polynomial function, for example, $a^- = 1, a^+ = R$ $(R > 0)$. Suppose $u_{\xi^*} = \bar{u}^*$; then we obtain the relations

$$a^- \frac{1 - \bar{u}^*}{-1 - \xi^*} = a^+ \frac{\bar{u}^* - 0}{\xi^* - 1}.$$

Then we obtain $\bar{u}^*$:

$$\bar{u}^* = \left(\frac{a^-}{1 + \xi^*} + \frac{a^+}{1 - \xi^*}\right)^{-1} \frac{a^-}{1 + \xi^*} = \frac{a^-(1 - \xi^*)}{a^-(1 - \xi^*) + a^+(1 + \xi^*)} = \frac{1 - \xi^*}{1 + R + (R - 1)\xi^*} \tag{8}$$

and

$$\tilde{N}_1(x) = \begin{cases} \frac{\bar{u}^* - 1}{\xi^* + 1}(\xi - \bar{u}^*) + \bar{u}^* & \text{if } \xi \leq \xi^*, \\ \frac{\bar{u}^*}{\xi^* - 1}(\xi - \bar{u}^*) + \bar{u}^* & \text{if } \xi > \xi^*, \end{cases} \tag{9}$$

which is different from $N_1(\xi) = (1 - \xi)/2$. We can also obtain $\tilde{N}_2(x)$ by defining

$$\hat{u}^* = \frac{R(1 + \xi^*)}{1 + R + (R - 1)\xi^*},$$

$$\tilde{N}_2(x) = \begin{cases} \frac{\hat{u}^*}{\xi^* + 1}(\xi - \hat{u}^*) + \hat{u}^* & \text{if } \xi \leq \xi^*, \\ \frac{\hat{u}^* - 1}{\xi^* - 1}(\xi - \hat{u}^*) + \hat{u}^* & \text{if } \xi > \xi^*. \end{cases} \tag{10}$$

To understand the $\tilde{N}_i(x)$, see Fig. 2.

We can also verify $\tilde{N}_1(\xi) + \tilde{N}_2(\xi) = 1$ in the reference element.

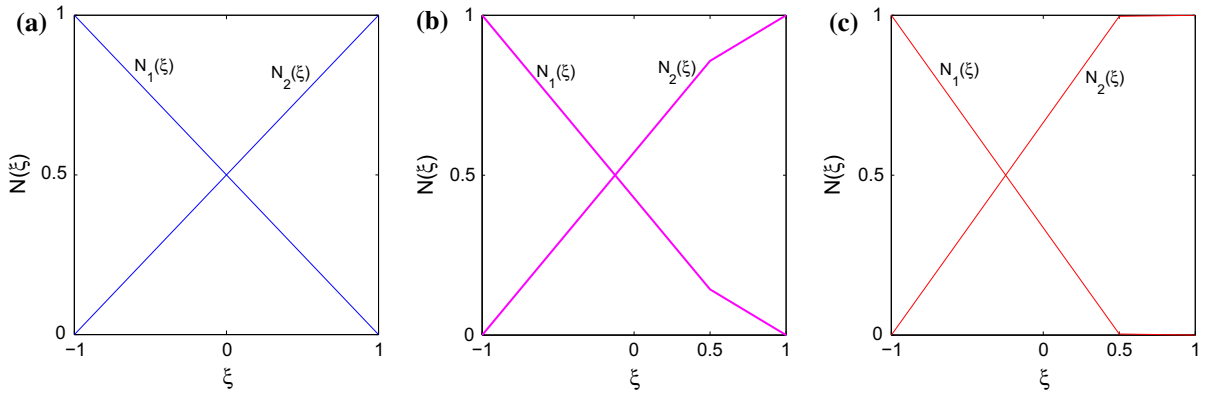

Fig. 2 Shape function $N(\xi)$ in reference element: **a** using standard FEM, **b** $R = 2$, $\xi^* = 1/2$ using intrinsic XFEM, **c** $R = 100$, $\xi^* = 1/2$ using intrinsic XFEM. (Color figure online)

If we use the simple Q_1 element, the shape function is a bilinear function. There are four shape functions with respect to the reference element $[-1, 1] \times [-1, 1]$:

$$\begin{cases} N_1(\xi,\eta) = \frac{(1-\xi)(1-\eta)}{4}, & N_2(\xi,\eta) = \frac{(1+\xi)(1-\eta)}{4}, \\ N_3(\xi,\eta) = \dfrac{(1+\xi)(1+\eta)}{4}, & N_4(\xi,\eta) = \frac{(1-\xi)(1+\eta)}{4}. \end{cases} \tag{11}$$

Suppose the interface passes through some elements as in Fig. 4:

$$\begin{cases} \tilde{N}_1(\xi,\eta) = \frac{(1-\xi)}{2} L_{14}(\eta), & \tilde{N}_2(\xi,\eta) = \frac{(1+\xi)}{2} L_{23}(\eta), \\ \tilde{N}_3(\xi,\eta) = \dfrac{(1+\xi)}{2} L_{32}(\eta), & \tilde{N}_4(\xi,\eta) = \frac{(1-\xi)}{2} L_{41}(\eta). \end{cases} \tag{12}$$

Here $L_{14}(\eta)$, $L_{23}(\eta)$, $L_{32}(\eta)$, $L_{41}(\eta)$ can be fixed by $\tilde{N}_1(\eta)$ and $\tilde{N}_2(\eta)$:

$$\begin{cases} L_{14}(\eta) = \tilde{N}_1(\eta) & \text{if } \eta^* = \eta_l, \\ L_{23}(\eta) = \tilde{N}_2(\eta) & \text{if } \eta^* = \eta_r, \\ L_{32}(\eta) = \tilde{N}_1(\eta) & \text{if } \eta^* = \eta_r, \\ L_{41}(\eta) = \tilde{N}_2(\eta) & \text{if } \eta^* = \eta_l, \end{cases} \tag{13}$$

where η^* denotes the intersection of interfaces on the reference element as in Fig. 4a, η_l is the y-coordinate of the left node in the reference element, and η_r is the y-coordinate of the right node in the reference element. Obviously, $\sum_{i=1}^{4} \tilde{N}_i(\xi,\eta) = 1$ always holds.

If the intersection of interfaces lies in ω_i, then the shape function should be modified at all nodes in that element. Here we use the more complicated basis of approximation around a fixed point $x \in \omega_i \subset \Omega$.

We present a specific example for a rectangle element. For example, the interface is each axis, and the intersection is the origin of the coordinate axes. The shape function in that element can be described as

$$\begin{cases} \tilde{N}_1(\xi,\eta) = L_{12}(\xi) L_{14}(\eta), & \tilde{N}_2(\xi,\eta) = L_{21}(\xi) L_{23}(\eta), \\ \tilde{N}_3(\xi,\eta) = L_{34}(\xi) L_{32}(\eta), & \tilde{N}_4(\xi,\eta) = L_{43}(\xi) L_{41}(\eta), \end{cases} \tag{14}$$

where $L_{i,j}(\xi)$ represents the ith node shape function related to the jth node in the x-direction on the reference element and $L_{i,j}(\eta)$ represents the ith node shape function related to the jth node in the y-direction on the reference element. For the interface problem, the intrinsic XFEM also uses a special shape function, which reflects the information of different interfaces, such as

$$\mathbf{p}^{\mathrm{T}} = \Big(1, x, y, |\phi_1(x)|, |\phi_2(x)|, |\phi_1(x)\phi_2(x)|\Big),$$

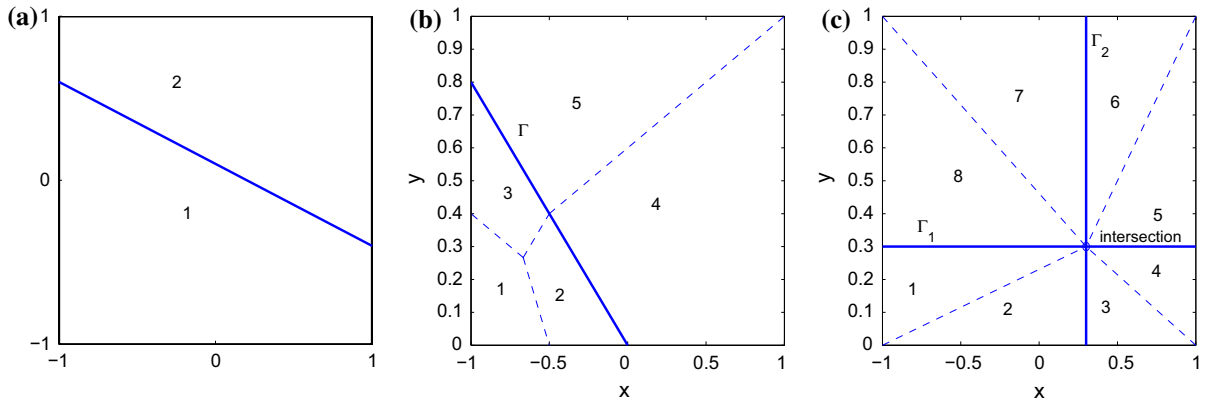

Fig. 3 Dividing a fully or partially cut element into i subelements: **a** $i = 2$, **b** $i = 5$, **c** $i = 8$. (Color figure online)

where ϕ_1 and ϕ_2 are level-set functions of two different interfaces. Then the intrinsic XFEM need to solve the weight function $\phi_i(x)$, matrix $M(x)$, and the inverse matrix of $M(x)$ in order to obtain the MLS function. If the matrix is singular, then there would be a computation and accuracy loss. And the intrinsic XFEM did not consider an interface in an intersection case.

The freedom that comes with the intrinsic XFEM is the same as that with the standard FEM. Actually, a finite element matrix is only changed at locations associated with intrinsically enriched nodes.

Remark 3.1 More generally, the problem is discontinuous across the interface $[u] \neq 0$ or the solution has singularity, such as $\nabla u|_{x_*} = \infty$ or $u|_{\tilde{x}} = \pm\infty$. The intrinsic XFEM can also be used to solve these problems. We should change the shape functions in domains near the interface and singularity nodes.

Remark 3.2 The immersed interface finite element method (IIFEM) proposed by Li [13] is still a special intrinsic XFEM; it uses triangulation and utilizes the connection of the discontinuity to construct a special basis function by which the element is cut by the interface.

4 Modified integration for intrinsic XFEM

Because of the existence of interfaces, the shape function may not be smooth in some elements, such as those cut by the interfaces. Therefore, we should adopt a modified integration instead of a Gaussian integration in these elements. Here we use the integration strategy of the XFEM [22,25].

In this work we first divide the special element by the interface (if the interface is a line), as shown in Fig. 3. The subelements may contain a triangle, a common quadrangle, or curved-edge graphics. In particular, if an element contains an intersection of interfaces (Fig. 4b), we should utilize the vertex of the element, the intersection of the edge and interface, or the intersection of different interfaces. To improve accuracy, the integration should use the same number of Gaussian nodes in the subdivision as in the ordinary elements.

If the interface Γ is curve and across any element by near or relative edge, then we should approximate it by some segments. This approximation leads to more subdivisions of domain Ω. For example, we use 5–7 segments in the (a)–(c) part of Fig. 4, respectively.

5 Numerical tests

We use MATLAB to implement our methods. First we introduce some notation:

SFEM: standard finite element method,

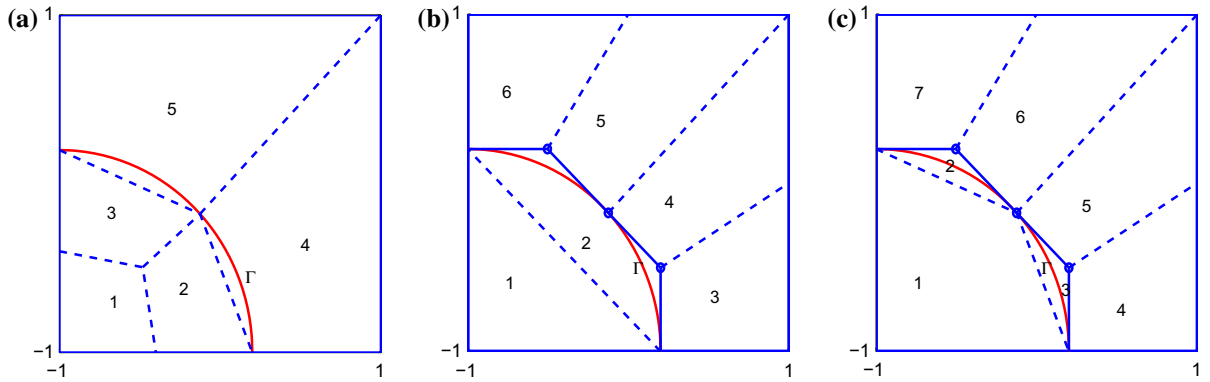

Fig. 4 Dividing a fully or partially cut element into i subelements: **a** $i = 5$, **b** $i = 6$, **c** $i = 7$. (Color figure online)

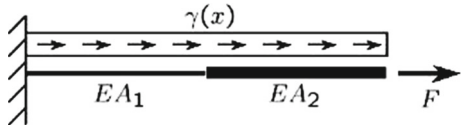

Fig. 5 Force bimaterial bar model

EXFEM: extrinsic extended finite element method,
IXFEM: intrinsic extended finite element method,
DOF: degrees of freedom,
$\|u - u_h\|_0$: relative L_2-error for u_h using IXFEM,
$\|u - u_h\|_{\varepsilon(\Omega)}$: relative energy error for u_h using IXFEM, defined by

$$\|u - u_h\|_{\varepsilon(\Omega)} = \left(\int_\Omega a(x, y)|\nabla(u - u_h)|^2 \,\mathrm{d}x\,\mathrm{d}y\right)^{1/2} \Big/ \left(\int_\Omega a(x, y)|\nabla u|^2 \,\mathrm{d}x\,\mathrm{d}y\right)^{1/2}.$$

In this section we choose two one-dimensional elliptic interface problems and the standard benchmark test used in some numerical results for an interface problem with intersecting interfaces used by many researchers [1].

Example 1 A bimaterial bar in one dimension is considered. A zero-displacement boundary is prescribed on the left. A horizontal line force and a point force on the right end is present. A sketch of the situation is shown in what follows. The exact displacement field features a kink, i.e., a weak discontinuity, where the material properties change. The mesh is incorporate for the discontinuity. That is, the kink is within an element and is captured using the XFEM (Fig. 5 and Table 1):

$$\frac{\mathrm{d}}{\mathrm{d}x}\left(k\frac{\mathrm{d}u}{\mathrm{d}x}\right) + \gamma(x) = F\delta(x - 1).$$

The exact solution is divided into two cases.
(a) There is a horizontal line force F_r on the right end [$\gamma(x) = 0$]:

$$u = \begin{cases} F_\mathrm{r}x/k_l & 0 \le x < \alpha, \\ F_\mathrm{r}(x - \alpha)/k_\mathrm{r} + F_\mathrm{r}\alpha/k_l & \alpha \le x \le 1. \end{cases} \tag{15}$$

(b) There is a point force on the right end (F_r):

$$u = \begin{cases} -(x - \alpha)^2/(2k_l) - (x - \alpha)(k_\mathrm{r} - k_l)/(4k_l(k_l + k_\mathrm{r})) + (4k_l + 4k_\mathrm{r})^{-1} & 0 \le x < \alpha, \\ -(x - \alpha)^2/(2k_\mathrm{r}) - (x - \alpha)(k_\mathrm{r} - k_l)/(4k_\mathrm{r}(k_l + k_\mathrm{r})) + (4k_l + 4k_\mathrm{r})^{-1} & \alpha \le x \le 1. \end{cases} \tag{16}$$

Based on the discontinuity at $x = \alpha$, k is discontinuous, $k = k_l$, if $x \le \alpha$, and $k = k_\mathrm{r}$ if $x > \alpha$. We can obtain a numerical solution using a modified IXFEM. If the numerical method is two-order accurate, its error will be machine errors. The numerical result of Example 1(a) verifies this argument. The numerical errors and orders of Example 1(b) are shown in Table 2. We use element P1, and the order of the L_2-error is greater than 2 (Fig. 6).

Table 1 Comparison of L_2-error using modified IXFEM and SFEM for Example 1, $\alpha = 0.5$

$1/h$	Example 1(a) $\|u - u_h\|_0$	Example 1(b) $\|u - u_h\|_0$	Orders
10	$2.93342140 \times 10^{-14}$	$7.58025222 \times 10^{-4}$	–
40	$4.37334270 \times 10^{-13}$	$4.21349229 \times 10^{-5}$	2.8898
160	$2.17641358 \times 10^{-12}$	$2.55844850 \times 10^{-6}$	2.8015
640	$2.94797212 \times 10^{-10}$	$1.58757579 \times 10^{-7}$	2.7798

Table 2 DOF, the L_2-errors for Example 2 using modified IXFEM and EXFEM

$1/h$	DOF	$\|u - u_{\text{IXFEM}}\|_0 + \|v - v_{\text{IXFEM}}\|_0$	$\text{DOF}_{\text{EXFEM}}$	$\|u - u_{\text{EXFEM}}\|_0 + \|v - v_{\text{EXFEM}}\|_0$
20	400	6.3756×10^{-3}	441	1.3949×10^{-2}
40	1600	1.7097×10^{-3}	1681	5.7955×10^{-3}
80	6400	4.1782×10^{-4}	6561	8.1636×10^{-3}
160	25,600	1.0664×10^{-4}	25,921	1.6681×10^{-3}

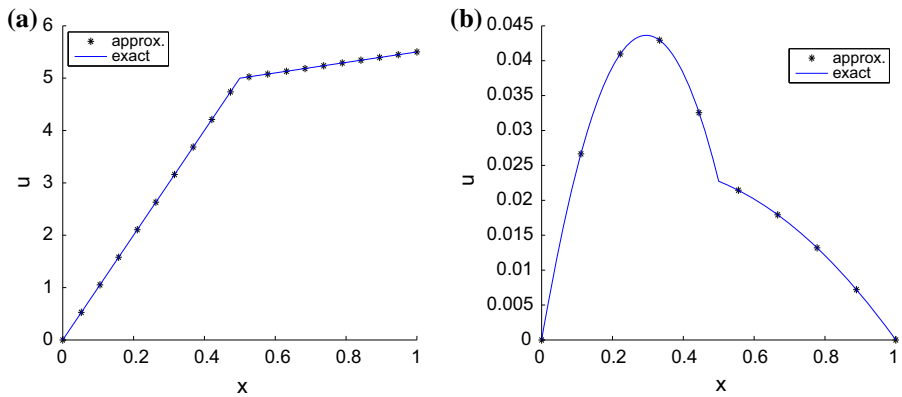

Fig. 6 Numerical solution and exact solution: **a** Example 1(a), **b** Example 1(b) $h = 0.1$

Example 2 Here we consider the linear elastostatic governing equations

$$\begin{cases} \nabla \cdot \sigma + \mathbf{b} = 0 \text{ in } \Omega, \\ \sigma = \mathbf{C} : \varepsilon, \\ \varepsilon = \nabla_s \mathbf{u}. \end{cases} \tag{17}$$

We use a modified intrinsic XFEM to carry out a two-dimensional solid test, considering the $\Omega = [0, 1] \times [0, 1]$, with the material interface $\Gamma : x^2 + y^2 = a^2 = 0.1608$. Let $E_1 = 100$, $\nu_1 = 0$ in $\Omega_1 = \left\{(x, y) \in \Omega | x^2 + y^2 \leq 0.404^2\right\}$ and setting $E_2 = 10$, $\nu_2 = 0$ in $\Omega_2 = \left\{(x, y) \in \Omega | x^2 + y^2 > \frac{1}{4}\right\}$, where $E_i, \nu_i (i = 1, 2)$ are Young's modulus and Poisson's ratio, respectively.

Moreover, let the area force $f_x = f_y = 0$ in the whole domain.

We use the notation $r = \sqrt{x^2 + y^2}$, $\mathbf{u} = (u, v)^{\mathrm{T}}$, and $\tan\theta = \frac{y}{x}$. Using the elastic equation, the exact solution is

$$\begin{cases} u = \frac{a}{8\mu}\left(\frac{r}{a}(\kappa + 1)\cos\theta + 2\frac{a}{r}((1 + \kappa)\cos\theta + \cos 3\theta) - 2\frac{a^3}{r^3}\cos 3\theta\right), \\ v = \frac{a}{8\mu}\left(\frac{r}{a}(\kappa - 3)\sin\theta + 2\frac{a}{r}((1 - \kappa)\sin\theta + \sin 3\theta) - 2\frac{a^3}{r^3}\sin 3\theta\right). \end{cases}$$

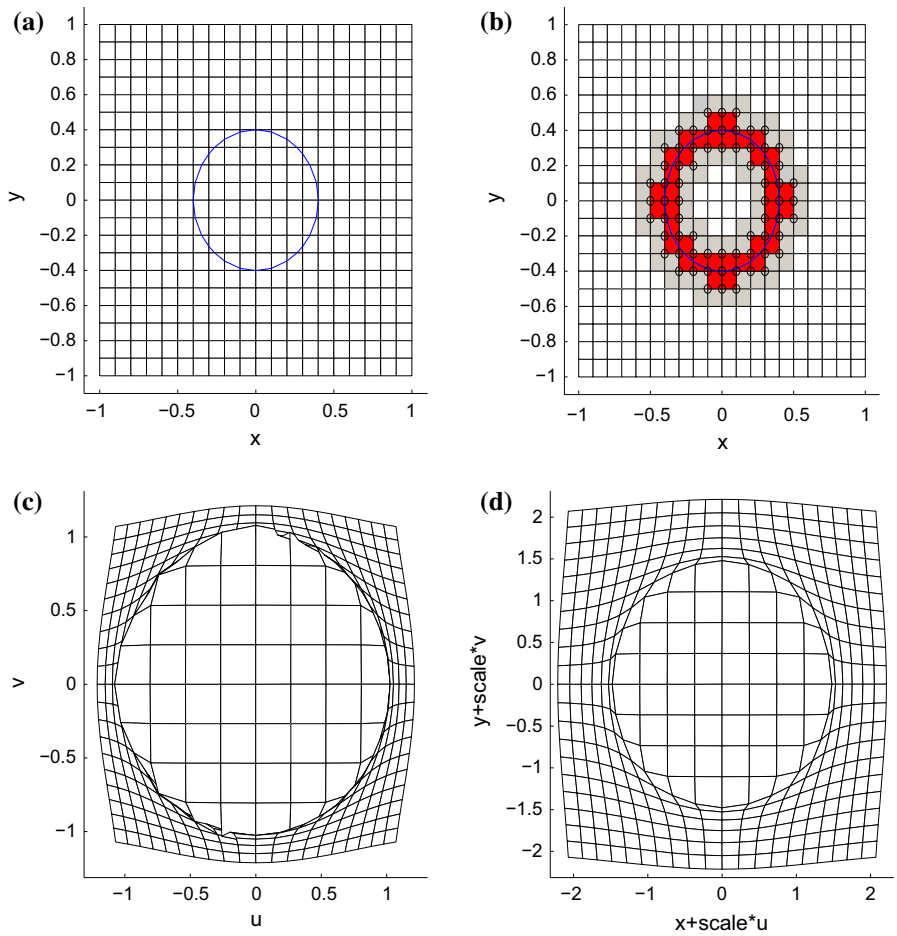

Fig. 7 Example 2 using modified IXFEM: **a** mesh and interface; **b** domain decomposed into three types by different *colors*; **c** u and v; **d** numerical result on elastic deformation. (Color figure online)

The result is shown in Table 2 and Fig. 7. It can be easily found that the DOF of the stiff matrix and the L_2-error is quite different between the modified IXFEM and the EXFEM. The error order is approximately 2 in the L_2 norm.

Example 3 Let $\Omega = (-1, 1) \times (-1, 1)$; the exact solution is

$$u(r, \theta) = r^{\beta}\mu(\theta)$$

in polar coordinates at the origin, with

$$\mu(\theta) = \begin{cases} \cos\left(\beta\left(\frac{\pi}{2} - \sigma\right)\right)\cos\left(\beta\left(\theta - \frac{\pi}{2} + \rho\right)\right) & \text{if } \theta \in [0, \frac{\pi}{2}], \\ \cos(\beta\rho)\cos(\beta(\theta - \pi + \sigma)) & \text{if } \theta \in \left(\frac{\pi}{2}, \pi\right], \\ \cos(\beta\sigma)\cos(\beta(\theta - \pi - \rho)) & \text{if } \theta \in \left(\pi, \frac{3\pi}{2}\right], \\ \cos\left(\beta\left(\frac{\pi}{2} - \rho\right)\right)\cos\left(\beta\left(\theta - \frac{3\pi}{2} - \sigma\right)\right) & \text{if } \theta \in (\frac{3\pi}{2}, 2\pi], \end{cases}$$

where ρ and σ are constant numbers. The exact solution satisfies (1), $f = 0$, and $a(x, y) = R$ if $(x, y) \in (0, 1)^2 \cup (-1, 0)^2$ and $a(x, y) = 1$ if $(x, y) \in \Omega\backslash([0, 1]^2 \cup [-1, 0]^2)$. The numbers β, R, σ, and ρ satisfy the nonlinear relations (e.g., [30,31])

$$R \approx 161.4476387975881, \rho = \pi/4 \quad \text{and} \quad \sigma \approx 14.92256510455152,$$

Table 3 DOF, condition of stiff matrix by FEM, modified IXFEM, and EXFEM

$1/h$	DOF	Cond_{FEM}	$\text{Cond}_{\text{IXFEM}}$	$\text{DOF}_{\text{EXFEM}}$	$\text{Cond}_{\text{EXFEM}}$
10	10	3.29891×10^3	1.0475×10^4	441	3.6304×10^4
40	1600	2.33598×10^4	2.4677×10^4	1681	2.84422×10^6
79	6400	9.83824×10^4	1.0091×10^5	6561	3.90791×10^9
159	25,600	4.03392×10^5	4.0835×10^5	25,921	1.27758×10^{11}

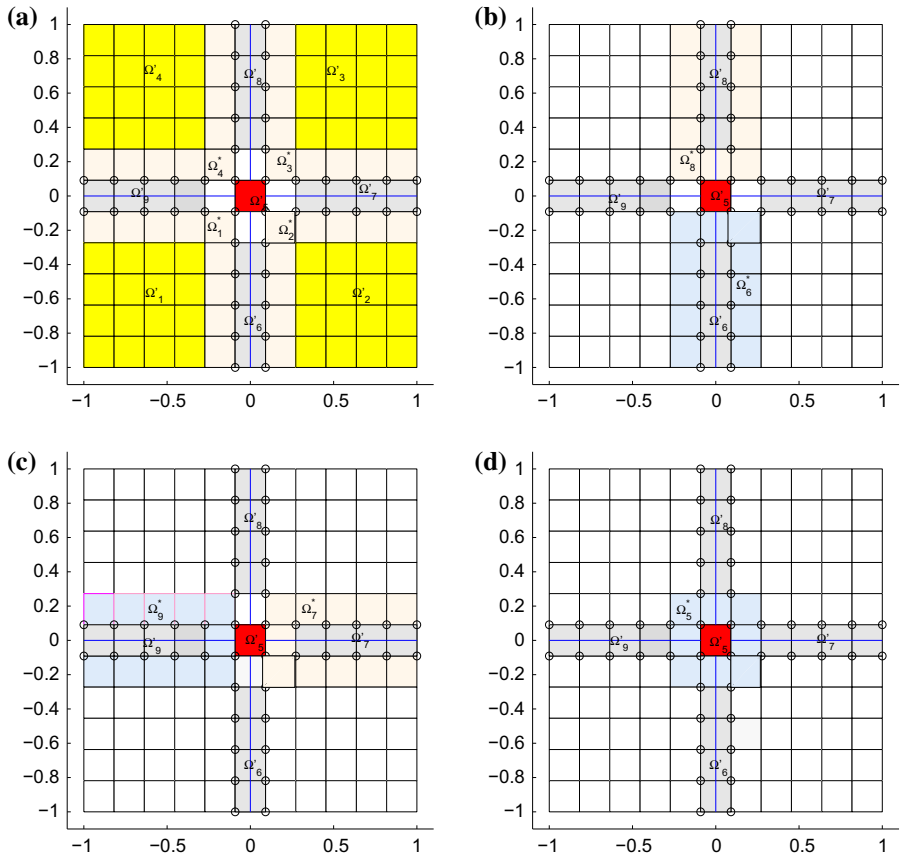

Fig. 8 Decomposition of domain Ω into subdomains $\Omega_l = \Omega_l' \cup \Omega_l^*$, Γ are four *blue lines*. Here $1 \le l \le 9$. (Color figure online)

where $\beta = 0.1$; this is a difficult problem for computation using the standard FEM. The exact solution is singular on the origin node and the interfaces Γ are the x-axis and y-axis [fixed by the discontinuity of $a(x, y)$]. $\Gamma_1 : \{(x, y)|xy = 0, x \ge 0\}$, $\Gamma_2 : \{(x, y)|xy = 0, y \ge 0\}$, $\Gamma_3 : \{(x, y)|xy = 0, x \le 0\}$, and $\Gamma_4 : \{(x, y)|xy = 0, y \le 0\}$. The origin node $(0, 0)$ is the intersecting interfaces (Table 3).

In this test we use a bilinear element, and divide the whole nodes into three different types. The division is showed in Fig. 8.

1. The ordinary nodes are x_i, $x_i \in \Omega_l'$, $l = 1, 2, 3, 4$, and their shape functions are unchanged.
2. The first enriched nodes are x_i^1, $x_i^1 \in \Omega_l'$, $l = 6, 7, 8, 9$, and their shape functions are partly changed in the x-direction or the y-direction.
3. The second enriched nodes are $x_i^2, x_i^2 \in \Omega_5'$, and their shape functions are changed in both the x- and y-directions.

Table 4 DOF, condition of stiff matrix by FEM, modified IXFEM, and EXFEM

$2/h$	DOF	$\text{Cond}_{\text{SFEM}}$	$\text{Cond}_{\text{IXFEM}}$	$\text{DOF}_{\text{EXFEM}}$	$\text{Cond}_{\text{EXFEM}}$
19	400	1.01906×10^4	1.0475×10^4	441	3.6304×10^4
39	1600	2.33598×10^4	2.4677×10^4	1681	2.84422×10^6
79	6400	9.83824×10^4	1.0091×10^5	6561	3.90791×10^9
159	25,600	4.03392×10^5	4.0835×10^5	25,921	1.27758×10^{11}

Table 5 Comparison of L_2-error using modified IXFEM and SFEM

$2/h$	DOF	IXFEM		SFEM	
		$\|u - u_h\|_0$	Order	$\|u - u_h\|_0$	Order
19	400	$5.85229689 \times 10^{-4}$	–	$1.29367331 \times 10^{-2}$	–
39	1600	$1.31518929 \times 10^{-4}$	2.1537	$6.11857595 \times 10^{-3}$	1.4541
79	6400	$3.12260721 \times 10^{-5}$	2.0745	$2.97964019 \times 10^{-3}$	1.4329
159	25,600	$7.61075872 \times 10^{-6}$	2.0366	$1.47079316 \times 10^{-3}$	1.4233
319	102,400	$1.87886932 \times 10^{-6}$	2.1722	$7.30756777 \times 10^{-4}$	1.4186

Table 6 Comparison of H_1-error ($\|u - u_h\|_{\varepsilon(\Omega)}$) using SFEM and modified IXFEM

$2/h$	IXFEM		SFEM	
	$\|u - u_h\|_{\varepsilon(\Omega)}$	Order	$\|u - u_h\|_{\varepsilon(\Omega)}$	Order
19	$2.88822559 \times 10^{-2}$	–	$2.88876285 \times 10^{-2}$	–
39	$1.36756549 \times 10^{-2}$	1.0786	1.9258×10^{-2}	0.5850
79	$6.66191543 \times 10^{-3}$	1.0376	1.3467×10^{-2}	0.5161
159	$3.28872591 \times 10^{-3}$	1.0184	9.4512×10^{-3}	0.5112
319	$1.63401288 \times 10^{-3}$	1.0091	6.6192×10^{-3}	0.5106

We list the numerical result in tables. In Table 4, the condition numbers of stiff matrices are compared. We easily find that the intrinsic XFEM still has the same order with the increased number of degrees of freedom. Table 5 shows the L_2-error and the rate of convergence obtained with the FEM and the modified IXFEM for the test. It is found that order 2 in the L_2-norm is obtained by using the modified IXFEM, while order 1.4 is obtained by using the standard FEM. It may be seen that a reduced convergence of 0.5 occurs due to the discontinuity when we use the standard FEM. It can be seen in Table 6 that for the proposed method the convergence is 1 in the energy norm, while the convergence is 0.5 for the FEM. To compare the nodal error in the whole domain, we give the error distribution by the FEM and the IXFEM in Fig. 9. It is obvious that the IXFEM decreases the error around the interfaces.

Compared with the extrinsic XFEM and SFEM, the modified intrinsic XFEM has the following properties:

1. Enrichment is realized locally where it is needed in the IXFEM, as in the extrinsic XFEM. Here we do not use enrichment intrinsic but rather modify the shape function instead of the MLS function.
2. The enrichment is realized intrinsically, without introducing additional unknowns. This is the most important difference from the extrinsic XFEM.

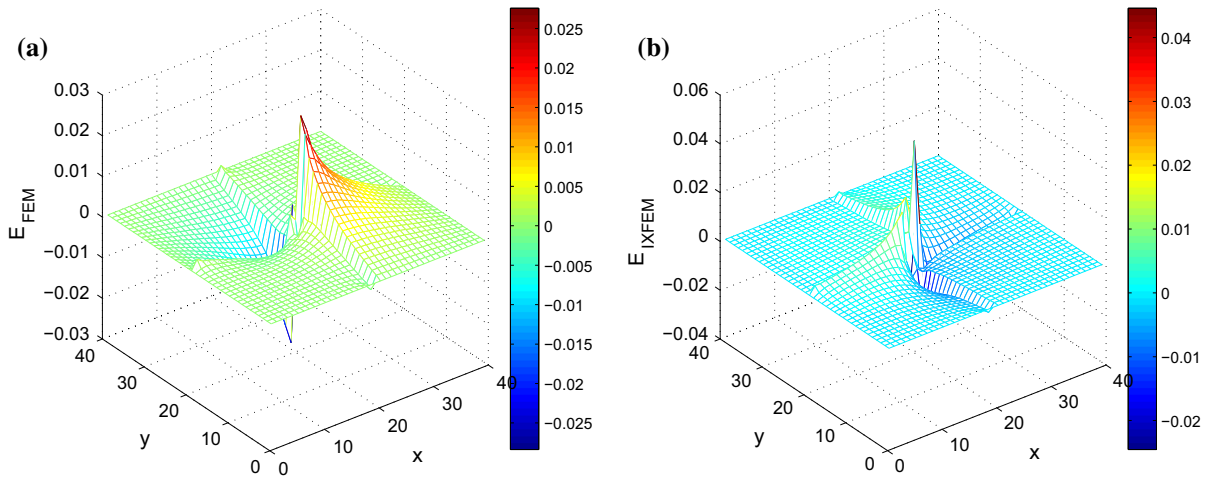

Fig. 9 Error distribution: **a** SFEM, **b** modified IXFEM $h = 2/39$

3. The condition number of the final system matrix scales with the same order over the element size as the SFEM for arbitrary enrichments. In the extrinsic XFEM, however, the condition number may significantly increase with refinement, which depends on a partial enrichment.
4. The increased amount of computational work for the intrinsic XFEM compared with the SFEM lies in the evaluation of the MLS functions. The number of enrichment functions added to the intrinsic basis is directly related to the computational burden in computing the MLS functions. Our method uses the modified function only in critical subdomains.

6 Conclusions

In this article, an intrinsic XFEM for the second-order elliptic equation with discontinuous coefficients and interfaces was discussed. The following conclusions may be drawn. First, we modified the local enrichment function space. The shape functions on critical subdomains are special functions that reflect the discontinuous information of the interface. Obviously, they differ from the MLS functions in the traditional intrinsic XFEM. Second, the condition number of the stiff matrix has the same order as the SFEM, while the extrinsic XFEM obtains an ill-conditioned system. This method can be extended to the general area and uses different meshes and high-order polynomials. Finally, a numerical simulation was given for the standard benchmark example. Numerical results give an L_2-error, an energy error, and their convergence orders. We obtained the convergence where $\|u - u_h\|_0$ is $O(h^2)$, and $\|u - u_h\|_{\varepsilon(\Omega)}$ is $O(h)$ when a bilinear element is used. Thus, the modified intrinsic XFEM is better than the SFEM. Of course, this method can be used in the future in many other interface problems, especially those containing intersections.

Acknowledgments This work was supported by the China Postdoctoral Science Foundation project (2014M562487) and the National Natural Science Foundation of China (11461068, 11171269, 11401332, 61163027, 11362021).

References

1. Cai Z, Zhang S (2009) Recovery-based error estimator for interface problems: conforming linear elements. SIAM J Numer Anal 47(3):2132C–2156
2. Bernardi C, Verfürth R (2000) Adaptive finite element methods for elleptic eqautions with non-smooth coefficients. Numer Math 85:579–608

3. Peskin CS (1977) Numerical analysis of blood flow in heart. J Comput Phys 25:220–252
4. Leveque RJ, Li ZL (1994) The immersed interface method for elleptic equations with discontinuous coefficients and sigular sources. SIAM J Numer Anal 31(4):1019–1044
5. Fogelson AL, Keener JP (2000) Immersed interface methods for Neumann and related problems in two and three dimensions. SIAM J Sci Comput 22:1630–1684
6. Li ZL, Ito K, Lai MC (2007) An augmented approach for Stokes equations with a discontinuous viscosity and singular forces. Comput Fluids 36:622–635
7. Huang H, Li ZL (1999) Convergence analysis of the immersed interface method. IMA J Numer Anal 19:583–608
8. Wiegmann A, Bube KP (2000) The explicit-jump immersed method: finite difference methods for PDEs with piecewise smooth solutions. SIAM J Numer Anal 37(3):827–862
9. Berthelsen PA (2004) A decomposed immersed interface method for variable coefficient elliptic equations with non-smooth and discontinuous solutions. J Comput Phys 197:364–386
10. Zhou YC, Zhao S, Feig M, Wei GW (2006) High order matched interface and boundary method for elliptic equations with discontinuous coefficients and singular sources. J Comput Phys 213:1–30
11. Pan KJ, Tan YJ, Hu HL (2010) An interpolation matched interface and boundary method for elliptic interface problems. J Comput Appl Math 234:73–94
12. Zhao JP, Hou YR, Li YF (2012) Immersed interface method for elliptic equations based on a piecewise second order polynomial. Comput Math Appl 63:957–965
13. Li ZL (1998) The immersed interface method using a finite element formulation. Appl Numer Math 27:253–267
14. Xie H, Li ZL, Qiao ZH (2011) A finite element method for elasticity interface problems with locally modified triangulations. Int J Numer Anal Model 8(2):189–200
15. He XM, Lin T, Lin YP (2011) Immersed finite element methods for elliptic interface problems with non-homogeneous jump conditions. Int J Numer Anal Model 8(2):284–301
16. Belytschko T, Black T (1999) Elastic crack growth in finite elements with minimal remeshing. Int J Numer Methods Eng 45:601–620
17. Moës N, Dolbow J, Belytschko T (1999) A finite element method for crack growth without remeshing. Int J Numer Methods Eng 46:131–150
18. Sukumar N, Chopp DL, Moës N, Belytschko T (2001) Modeling holes and inclusions by level sets in the extended finite-element method. Comput Methods Appl Mech Eng 190:6183–6200
19. Chessa J, Wang H, Belytschko T (2003) On the construction of blending elements for local partition of unity enriched finite elements. Int J Numer Methods Eng 57:1015–1038
20. Moës N, Cloirec M, Cartraud P, Remacle JF (2003) A computational approach to handle complex microstructure geometries. Comput Methods Appl Mech Eng 192:3163–3177
21. Ji H, Dolbow JE (2004) On strategies for enforcing interfacial constraints and evaluating jump conditions with the extended finite element method. Int J Numer Methods Eng 61:2508–2535
22. Fries TP, Belytschko T (2010) The extended-generalized finite element method—an overview of the method and its applications. Int J Numer Methods Eng 84(3):253–304
23. Belytschko T, Gracie R, Ventura G (2009) A review of extended/generalized finite element methods for material modeling. Model Simul Mater Sci Eng 17:1–24
24. Wu JY (2011) Unified analysis of enriched finite elements for modeling cohesive cracks. Comput Methods Appl Mech Eng 200:3031–3051
25. Fries TP, Belytschko T (2006) The Intrinsic XFEM: a method for arbitrary discontinuities without additional unknowns. Int J Numer Methods Eng 68:1358–1385
26. Vaughan BL, Bryan J, Smith G, Chopp DL (2006) A comparison of the extended finite element method with the immersed interface method for elliptic equations with discontinuous coefficients and singular sources. Commun Appl Math Comput Sci 1(1):207–228
27. Strouboulis T, Copps K, Babuška I (2000) The generalized finite element method: an example of its implementation and illustration of its performance. Int J Numer Methods Eng 47:1401–1417
28. Babuška I, Banerjee U (2012) Stable generalized finite element method (SGFEM). Comput Methods Appl Mech Eng 201:91–111
29. Babuška I, Melenk JM (1997) The partition of unity method. Int J Numer Methods Eng 40:727–758
30. Kellogg RB (1975) On the poisson equation with intersecting interfaces. Appl Anal 4:101–129
31. Morin P, Nochetto RH, Siebert KG (2002) Convergence of adaptive finite element methods. SIAM Rev 44:631–658